

# Second-Harmonic Generation of Spoof Surface Plasmon Polaritons Using Nonlinear Plasmonic Metamaterials

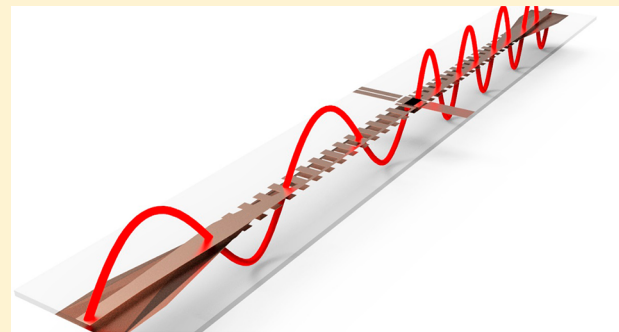
Hao Chi Zhang,<sup>†</sup> Yifeng Fan,<sup>†</sup> Jian Guo,<sup>†</sup> Xiaojian Fu,<sup>†</sup> and Tie Jun Cui<sup>\*,†,‡</sup>

<sup>†</sup>State Key Laboratory of Millimeter Waves, Southeast University, Nanjing 210096, China

<sup>‡</sup>Cooperative Innovation Centre of Terahertz Science, No. 4, Section 2, North Jianshe Road, Chengdu 610054, China

**ABSTRACT:** Second-harmonic generation is one of the most important applications of nonlinear effects, which has attracted great interest in nonlinear optics and microwaves in the past decades. Here, the second harmonics of spoof surface plasmon polaritons (SPPs) are generated with high efficiency at microwave frequencies using a subwavelength-scale nonlinear active device that is integrated on specially designed plasmonic waveguides. Composed of two ultrathin corrugated metallic strips printed on the top and bottom surfaces of a thin dielectric slab antisymmetrically, the plasmonic waveguide supports broadband propagations of spoof SPPs with a strong subwavelength effect, whose dispersion property can be controlled by changing the geometrical parameters. By loading the nonlinear device to the intersection of two plasmonic waveguides with different corrugation depths, the efficient generation of second-harmonic SPPs is experimentally demonstrated in the broad frequency band. The proposed second-harmonic generator is directly used as an SPP frequency multiplier, and the proposed method can be extended to achieve high-order harmonics, which are essential to SPP integrated circuits and systems.

**KEYWORDS:** *spoof surface plasmons, nonlinear, second-harmonic generation, nonlinear metamaterials*



**A**t optical frequencies, natural surface plasmon polaritons (SPPs) are special surface electromagnetic (EM) waves, which crawl along the interface between metal and dielectric materials. SPPs have spurred great interest in physics during the past decades due to the potential for developing new types of photonic devices.<sup>1,2</sup> The interactions between free electrons of a conductor and surrounding EM fields give rise to unique properties of SPPs, such as the significant field confinement in the vicinity of a metal–dielectric interface and great enhancement of EM fields.<sup>3–7</sup> Motivated by recent advances that allow metals to be structured and characterized on the nanometer scale, SPPs have found promising applications in super-resolution imaging,<sup>8–11</sup> miniaturized sensors,<sup>12,13</sup> photovoltaics,<sup>14</sup> graphene-based devices,<sup>15</sup> photolithography,<sup>16</sup> etc. The SPP-based optical circuits have been considered as a solid venue for future developments.<sup>17</sup>

However, SPPs cannot be supported directly at microwave and terahertz frequencies because metals fundamentally act as perfect electric conductors below the far-infrared regime, instead of plasmas with a negative permittivity. In order to achieve highly confined SPPs at lower frequencies, plasmonic metamaterials have been proposed,<sup>18–29</sup> whose performance can be designed at will through changing the geometrical parameters of surface structures. Spoof SPPs have inherited the most exotic features of optical SPPs, such as field confinement and nondiffraction limit. Recently, an ultrathin corrugated metallic strip has been proposed to propagate conformal surface plasmons (CSPs) on arbitrarily curved surfaces,<sup>30</sup> which

represents one of the most promising candidates for applications of SPP devices and circuits at microwave and terahertz frequencies owing to the ultrathin structure, low loss, broad bandwidth, and great flexibility.

The strong EM fields resulting from SPPs allow a weakly nonlinear process, which depends linearly on the local fields.<sup>31</sup> In previous studies, nonlinear media have been employed to enhance the nonlinear effects,<sup>32–38</sup> such as nonlinear crystals in the optical regime and split-ring resonators with packaged varactors embedded in capacitive gaps in the microwave regime.<sup>32</sup> Since electrically large and bulky nonlinear media are required, it is difficult to realize compact and efficient SPP nonlinear devices. More importantly, the required large intensity of incident waves to excite the nonlinear phenomena is much stronger than that used in applications (e.g., communications and sensing), which makes it more difficult to realize high-efficiency nonlinear SPP devices.

As one of the most important applications of nonlinear effects, second-harmonic generation has attracted great interest in nonlinear optics and microwaves in the past decades. However, most of the previous studies involving nonlinear surface plasmons were aimed at controlling spatial lights or EM waves by the enhanced nonlinear effects,<sup>39–41</sup> and only a few works have demonstrated the second-harmonic generation of SPPs with low efficiency at optical frequencies.<sup>42</sup> To increase

**Received:** October 9, 2015

**Published:** December 22, 2015

the efficiency for the second-harmonic generation significantly, in this work, we propose to realize the second harmonics of spoof SPPs at microwave frequencies using semiconductor technology. Taking advantage of semiconductor technology in the microwave regime, we propose to use a nonlinear active chip on the subwavelength scale to produce high-order harmonics of spoof SPPs, as illustrated in Figure 1a. Our

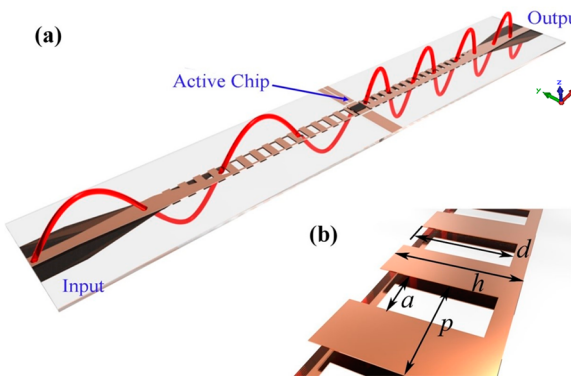


**Figure 1.** Second-harmonic generation of spoof SPPs. (a) Schematic diagram showing the generation of the second-harmonic SPPs through a subwavelength-scale nonlinear active chip integrated in a special plasmonic waveguide composed of two antisymmetrical metallic strips. (b) Detailed structure of the special plasmonic waveguide, in which the geometry configuration of a unit cell is described by the length  $p$ , groove depth  $d$ , groove width  $a$ , and strip width  $w$ .

purpose is not only to verify the physical phenomena of nonlinear SPPs but also to produce SPP frequency multipliers and mixers with high gain and high efficiency for real

applications. To integrate the subwavelength-scale nonlinear chip into the spoof SPP structures conveniently, we use a specially designed plasmonic waveguide,<sup>43</sup> which is constructed by printing two narrow corrugated metallic strips on the top and bottom surfaces of a thin dielectric substrate with mirror symmetry. Numerical simulations and experimental results demonstrate the efficient generation of second-harmonic SPP waves propagating along the plasmonic waveguides.

It has been shown that the ultrathin corrugated metallic strip is a good SPP transmission line at microwave and terahertz frequencies,<sup>30</sup> but it cannot be integrated with an active device due to the single-line structure. To solve the problem, a special plasmonic waveguide has been proposed, which is composed of two antisymmetrically corrugated metallic strips. The mirror structure is capable of connecting the active device efficiently and exhibits stronger subwavelength and field confinement effects. Figure 1b depicts the unit cell of the plasmonic waveguide, in which the groove depth and width are denoted as  $d$  and  $a$ , and the strip width and thickness are  $t$  and  $h$ , respectively. The whole structure is constructed by arranging such unit cells along the  $x$  axis with period  $p$  and its mirror duplicate on the top and bottom surfaces of a dielectric substrate with thickness  $t_s$ . We remark that the substrate can be designed as ultrathin and flexible,<sup>30</sup> if required.

It has been demonstrated that the equivalent plasmonic frequency of the mirror structure is much smaller than that of the single comb-shaped SPP waveguide<sup>30</sup> under the same geometrical configuration. We show that the mirror structure possesses more significant frequency dispersions than the single corrugated strip with the cutoff frequency decreasing rapidly. For specification, the dispersion curve of two antisymmetrically corrugated metallic strips deviates from the light line more

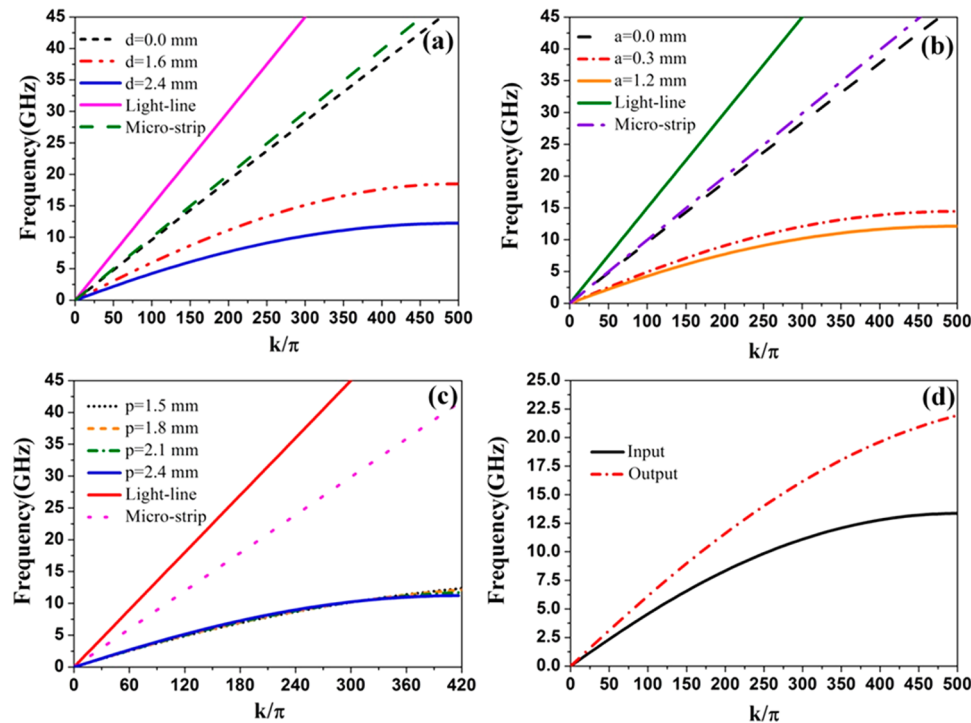


**Figure 2.** Dispersion diagrams of different plasmonic structures. (a) Plasmonic structures when the groove depth ranges from 0 to 2.4 mm. (b) Plasmonic structures when the groove width ranges from 0 to 1.2 mm. (c) Plasmonic structures when the period ranges from 1.5 to 2.4 mm. (d) Input and output plasmonic structures. Other parameters in all scenarios are fixed as  $h = 2.5$  mm,  $t = 0.018$  mm, and  $t_s = 0.5$  mm. The material types of metal and substrate are selected as copper and F4B.

significantly. This unique feature results in smaller propagating wavelength and tighter EM field confinements using the proposed SPP waveguide under the same frequency, predicting promising applications such as miniaturized SPP devices and low-interference transmission lines.

We consider two cases of the special plasmonic waveguide, which support spoof SPPs in two frequency bands. To accomplish the design, we investigate the dispersion properties of the mirror structures with different periods, groove depths, and widths. On the basis of the available metallic film and dielectric substrate, the geometrical parameters are chosen as  $h = 2.5$  mm,  $t = 0.018$  mm, and  $t_s = 0.5$  mm. The metal is selected as copper, and the dielectric substrate is F4B with relative permittivity  $\epsilon_r = 2.65$  and loss tangent  $\tan \delta = 0.001$ . We carry out the numerical simulations by the commercial software CST Microwave Studio. Figure 2a shows the dispersion curves of the mirror structure with fixed period and groove width ( $p = 2.0$  mm and  $a = 1.0$  mm) and varying groove depth  $d$ . We observe that the curve with  $d = 0$ , which corresponds to two parallel metal strips, is very similar to the dispersion curve of a traditional microstrip and is well distinct from the light line. As  $d$  increases from 0.8 to 2.4 mm, the dispersion curve deviates gradually from that of the microstrip and further from the light line and asymptotically approaches different cutoff frequencies. This is similar to the phenomenon originally appearing in the optical frequencies for natural SPPs.

We further investigate the influences of structure period and groove width on the wave momentum and cutoff frequency. When the period and groove depth are fixed ( $p = 2.0$  mm and  $d = 2.4$  mm) while the groove width  $a$  varies, the dispersion relations are illustrated in Figure 2b, in which the curve with  $a = 0$  again corresponds to two parallel metal strips. As  $a$  increases from 0.3 to 1.2 mm, the dispersion curve does not exhibit so significant changes as observed in Figure 2a, implying that the dispersion characteristic of the mirror structure is insensitive to the groove width. In this regard, the proposed plasmonic waveguide allows slightly tuning of wave momentum by adjusting the groove width. In Figure 2c, the groove depth and width are fixed as  $d = 2.4$  mm and  $a = 1.0$  mm. When the period  $p$  increases from 1.5 to 2.4 mm, the dispersion curve remains unchanged in the transmission band. However, the period influences the cutoff frequency slightly, and hence it is an effective approach to tune the cutoff frequency independently in small ranges by changing the period. This performance is caused by the fact that most EM fields are confined in the groove and dielectric. The dielectric thickness  $t_s$  and groove parameters (e.g., the groove depth  $d$  and groove width  $a$ ) play a determinative role in the cutoff frequencies, while the period  $p$  will affect the EM coupling between the two grooves and have a slight effect on the cutoff frequencies.

We optimize the geometries of the input and output plasmonic waveguides so as to cover the working bandwidth of the nonlinear active chip, and the optimized geometrical parameters are presented in Table 1. The corresponding dispersion curves of the input and output structures are

**Table 1. Geometrical Parameters of the Input and Output Plasmonic Waveguides**

	period $p$	groove width $a$	groove depth $d$
input waveguide	2.0 mm	1.0 mm	2.2 mm
output waveguide	1.5 mm	0.6 mm	1.5 mm

illustrated in Figure 2d. Owing to the easy tuning of the wave momentum, we design a smooth conversion between SPP waves and conventional guided waves.<sup>44</sup> The conversion part functions as the momentum matching and impedance matching between the traditional microstrip and the plasmonic waveguides.

In the past, nonlinear metamaterials have been proposed<sup>32</sup> in which a packaged varactor was embedded in the metamaterials to enhance the nonlinear effect. However, a powerful incident field was required, and hence the nonlinear phenomenon is hard to observe and difficult to apply in engineering.

To solve the problem, we propose to employ a field effect transistor (FET), which is a kind of active audion, to generate the second harmonics of spoof SPPs. The nonlinear effect of the FET is more significant than that of the packaged varactor, which makes it easier to generate high-order harmonics. More importantly, the output characteristics of the FET can be tuned by direct current (dc) bias, and this strategy is easily implemented by the semiconductor technology. If we use a single FET to generate the second-harmonic SPPs, the conversion gain is calculated analytically as

$$G = V_{2\text{-order}}/V_{\text{input}} = 2 \sum_{n=1}^{\infty} \frac{q^{(2n)}(V)}{(2n!!)^2} V_{\text{input}}^{2n-1} \frac{n}{n+1} \quad (1)$$

in which  $V_{\text{input}}$  is the amplitude of the input SPP signal,  $V$  is the dc bias, and  $q(\bullet)$  represents the voltage response function of the FET.

To achieve significant conversion gain and restrain other higher-order harmonics, we apply a simple FET model in our design, as illustrated in Figure 3a, which consists of a differential amplifier circuit that acts as an active balun. There is a 180° phase difference between the two outputs of the balun. Then the outputs feed the gates of balanced FETs, and the drains are connected to form the single-ended output, which results in the cancellation of fundamental frequency and odd harmonics and

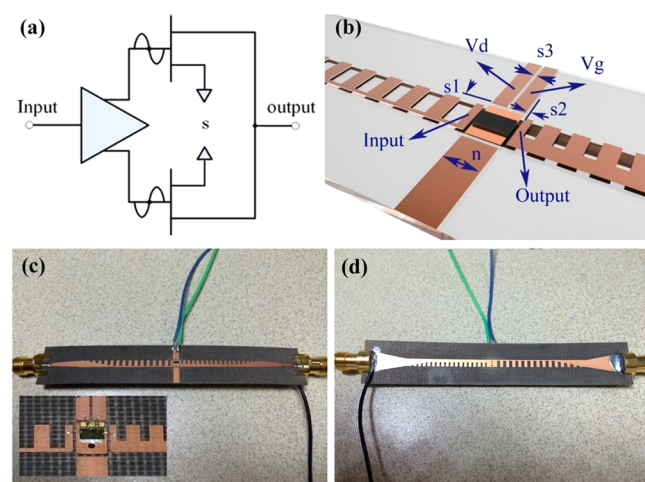


**Figure 3.** Design and fabrication of the second-harmonic spoof SPP generator. (a) Topology diagram of the proposed strategy to generate second-harmonic SPPs. (b) Top view of the installation section for a nonlinear active chip, in which  $n$  is the length of the central pad and  $S1$  and  $S2$  are the gaps between the central pad and the structures around it. (c, d) Photographs of the fabricated sample (top view and bottom view) of the second-harmonic SPP generator. The inset of (c) shows the enlarged view of the active chip mounted on the plasmonic waveguide.

the in-phase superposition of even-harmonic drain currents. In this figure, the node "S" represents a virtual ground.

For simplicity, we analyze this strategy using the circuit method. We assume that the input signal can be expressed as a function of angular frequency, while the dc bias remains the same in the process. The final output of the two FETs is calculated analytically as

$$\begin{aligned} V_{\text{out}} &= q(V + V_{\text{in}}(\omega)) + q(V - V_{\text{in}}(\omega)) \\ &= \sum_{n=1}^{\infty} \frac{2q^{(2n)}(V)}{2n!} V_{\text{in}}^{2n}(\omega) \end{aligned} \quad (2)$$

in which  $V_{\text{in}}(\omega)$  is the input SPP signal as a function of angular frequency. Since high-order terms exist, the nonlinear field is generated through the combination of two FETs. To obtain a certain harmonic, we can change the dc bias ( $V$ ) to make the FET work in an appropriate voltage range. Except the FETs, the whole system can be regarded as a linear system. According to the dispersion spectrum of spoof SPPs, the transmission spectrum of the SPP waveguide corresponds to a low-pass filter, which can effectively suppress the higher-order harmonics. The dispersion property of spoof SPPs, which can be engineered at will by changing the geometrical parameters, provides greater convenience to design functional devices than that of traditional transmission lines.

Hence we use two transmission-spectrum functions,  $A_1(\bullet)$  and  $A_2(\bullet)$ , to describe the response of the linear input part (including the input spoof SPP waveguide) and differential amplifier and the response of the linear output part (including the output SPP waveguide), respectively. For ease of understanding, we consider the simplest case, i.e., the single-frequency incidence. Then the conversion gains from the fundamental frequency to the second harmonic and the third harmonic are calculated analytically as

$$\begin{aligned} G &= V_{\text{2-order}}/V_{\text{input}} \\ &= 4A_2(2\omega) \sum_{n=1}^{\infty} \left( A_1^{2n}(\omega) V_{\text{input}}^{2n-1} \frac{q^{(2n)}(V)}{(2n!)^2} \frac{n}{n+1} \right) \end{aligned} \quad (3)$$

which indicates that the second harmonic is significantly enhanced, while the third harmonic is completely restrained. More importantly, the conversion gain is a function of the dc bias, implying that it is possible to modulate the second harmonic by changing the dc bias. Compared to the bulk nonlinear materials, the nonlinear plasmonic metamaterial structuring by the FET can easily support a tunable high-gain nonlinear process, due to the strong nonlinearity of the FET. On the other hand, owing to the significant field confinement and the single-mode transmission of the plasmonic waveguide, the second SPP harmonics can be generated with a high gain in a wide frequency band. In our scheme, the FET is excited by the equivalent voltage in the input plasmonic waveguide, and the next waveguide is excited by the output voltage. Hence in this scheme we do not need to consider the condition of phase matching, which may limit the operating frequency range.

To verify the generation of second SPP harmonics in microwave frequencies, we consider a realistic FET device in numerical simulations. Specifically, we choose a commercially available AMMC-6120 nonlinear active chip, which is commonly used in conventional active microwave devices and circuits, and the kernel is adaptive to our strategy. The other parts of AMMC-6120 can be regarded as a matching network

to the 50 ohm. We apply the AMMC-6120 active chip to produce the nonlinear second harmonics and control the input power at 1 mW. From the previous discussion, the SPP waveguide is an ideal filter. Hence the conversion gain is estimated as 12.6 from 5 to 10 GHz according to eq 3.

For quantitative analysis, we perform full-wave simulations using CST Microwave Studio. The whole structure is illustrated in Figure 1a, in which metal and substrate materials are selected as copper and F4B ( $\epsilon_r = 2.65$ ,  $\tan \delta = 0.001$ ). The geometrical parameters of input and output plasmonic waveguides are listed in Table 1. As shown in Figure 3b, the input, output, and dc bias pads of the AMMC-6120 chip are connected to points "input", "output", "Vd", and "Vg" on the double-sided plasmonic structure, respectively. The central pad, on which the chip is located, is connected to the bottom metallic strip via holes. As a consequence, the chip and plasmonic waveguide share the same ground, which is essentially impossible for the single-sided SPP waveguide.<sup>30</sup> All geometrical parameters of the structure around the chip have been carefully optimized to guarantee good impedance matching, which enables the EM energy to bump into and flow out of the chip efficiently. We define the input and output of the active chip as ports 2 and 3, and the input and output of the whole structure as ports 1 and 4, respectively. The simulated S parameters of the structure are illustrated in Figure 4a, in which  $S_{41}$  shows that almost no energy flows to the output port directly,  $S_{21}$  indicates that most of the input energy transfers to the input of the active chip through the input plasmonic waveguide, while  $S_{43}$  implies that

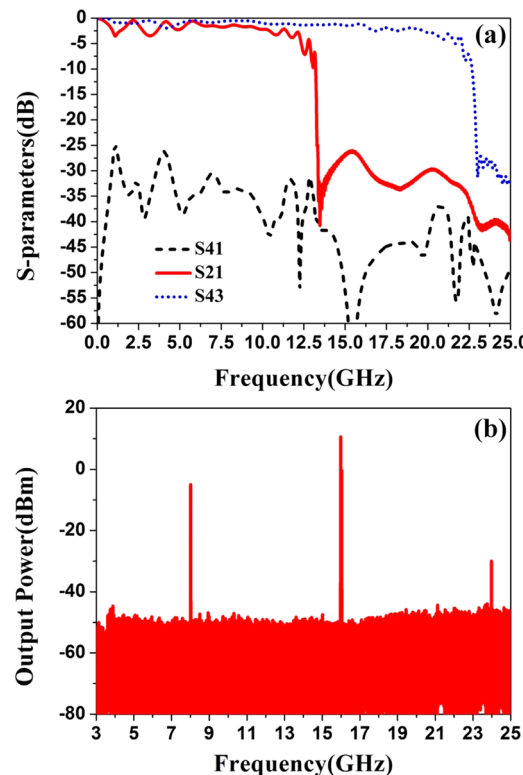


**Figure 4.** Simulation and measurement results of the second-harmonic SPP generator. (a) Simulated scattering S parameters of the whole structure, in which the input and output of the nonlinear active chip are replaced by two ports (3 and 4), in which the material types of metal and substrate are selected as copper and F4B. (b) Measured frequency spectrum of the second-harmonic SPP generator when the fundamental frequency is 8 GHz.

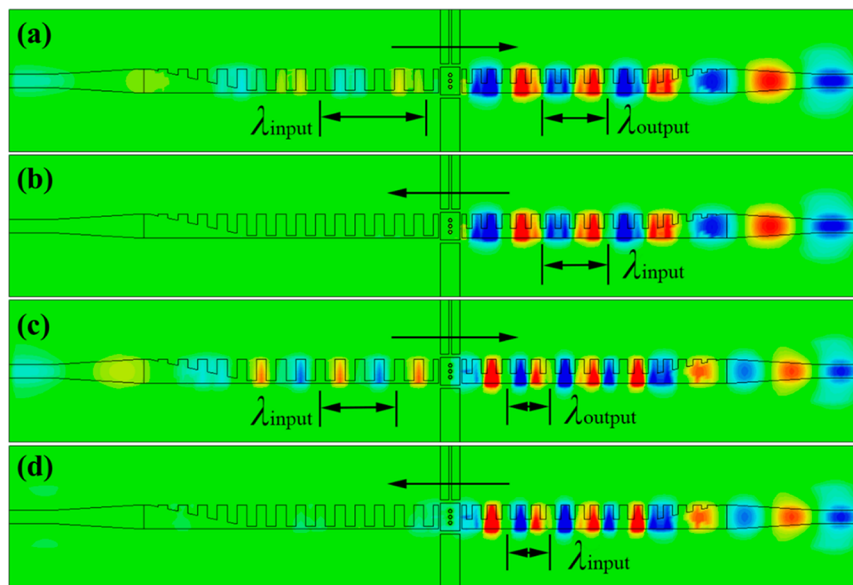


**Figure 5.** Simulated near-electric-field distributions on the plasmonic structure surface at different frequencies  $f$  and different signal directions, in which the black outline indicates the region of spoof SPP waveguides. (a)  $f = 8$  GHz and forward direction. (b)  $f = 16$  GHz and reverse direction. (c)  $f = 10$  GHz and forward direction. (d)  $f = 20$  GHz and reverse direction.

most of the second-harmonic energy transfers to the output port through the output plasmonic waveguide.

For direct observation of the field distribution in the whole structure, we make a connection between ports 1 and 3. Figure 5 illustrates the electric-field distributions on the structure surface when the fundamental frequency is 8 and 10 GHz, which are jointed by the electric fields of the input waveguide at the fundamental frequency and output waveguide at the second-harmonic frequency. We clearly observe that the fundamental SPP modes on the input waveguide are efficiently converted to the second-harmonic SPP modes on the output waveguide with significant amplifications of the converted fields. Caused by the nonreciprocity of the FET, the proposed method has a good unidirectional performance, as shown in Figure 5b and d. We note that the fundamental SPP mode cannot be excited by inputting the second-harmonic SPP mode inversely. We also notice that both fundamental and second-harmonic SPP fields are tightly confined in deep-subwavelength scales around the waveguides with low propagation loss.

On the basis of the printed circuit board (PCB) technology, we fabricate a sample of active plasmonic waveguide with the same parameters as used in the aforementioned simulations, whose bottom and top views are illustrated in Figure 3c and d, respectively. The commercially available AMMC-6120 active chip is attached onto the central pad using electrically conductive adhesive. Each welding spot is connected to the corresponding unit cell on the structure using bonding wire, as shown in Figure 3b. To guarantee pure dc input, three bypass capacitors of 100 pF are added among the Vd and Vg pads on the plasmonic waveguide and the dc bias welding spot on the active chip. By welding two standard sub-miniature-A (SMA) type connectors to the two ports of the plasmonic waveguide, the frequency spectrum of the whole system is obtained by using an Agilent signal generator (E8257D) and Agilent spectrum analyzer (E4447A). The measured results are presented in Table 2. As a typical example, the measured frequency spectrum at 8 GHz is demonstrated in Figure 4b, from which the second harmonic is clearly observed at 16 GHz

**Table 2. Experimental Results in Generating the Second-Harmonic Spoof SPPs**

input frequency (input power: 1 mW)	first harmonic (mW)	second harmonic (mW)	third harmonic (mW)
5 GHz	0.0316	12.8825	0.4365
6 GHz	0.0200	10.0	0.2399
7 GHz	0.0251	9.1201	0.1660
8 GHz	0.3162	11.4815	0.001
9 GHz	0.5248	10.0	0.000 02
10 GHz	0.1380	10.4713	0.000 003

with significant gain, accompanying a very weak third harmonic at 24 GHz.

From Table 2, we note that the measured conversion gain from the fundamental frequency to the second harmonic is around 10 when the fundamental frequency changes from 5 to 10 GHz, which is very close to the theoretical prediction of 12.6. Hence the second-harmonic SPPs are efficiently generated in a wide frequency band under the current design. From the same table, we also observe small measured conversion gain from the fundamental frequency to the third harmonic, which is caused by the cutoff characteristic of the output plasmonic waveguide. The significant reduction of the third harmonic is one of distinctive advantages of SPPs over the traditional transmission lines. The small discrepancies between theoretical analysis and measured results may originate from the loss of the SPP waveguide, the assembling error, and the bonding wire effect in the experiments, which have not been considered in the previous analysis.

For direct observation of the field distribution in the whole structure, we measure the near electric fields on an observation plane at 1.5 mm above the active SPP structure. The traditional method of the near-field measurement system relies heavily on a vector network analyzer (VNA). But most VNAs are linear systems, which require the frequency of measured near fields be the same as the frequency of the input signal. To overcome this problem, we propose a new near-field measurement system,

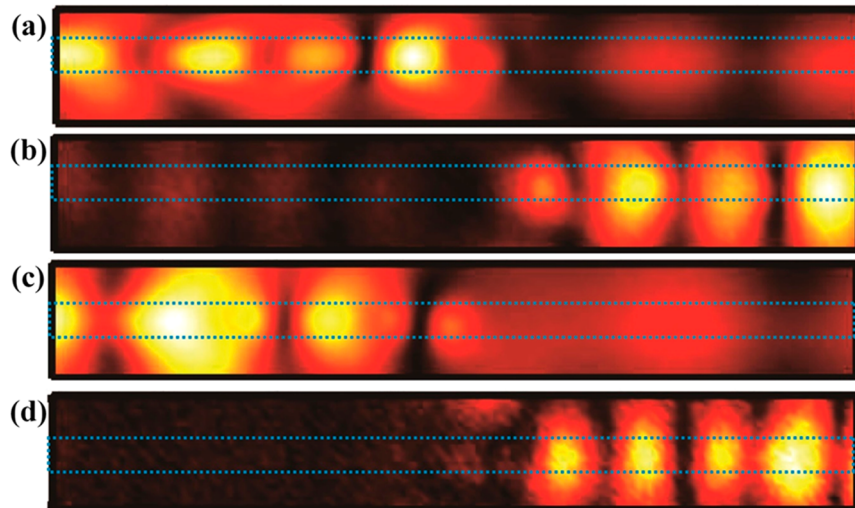


**Figure 6.** Measured near-electric-field distributions on the observation plane that is 1.5 mm above the plasmonic structure at different frequencies, in which the geometry parameters are shown in Table 1. (a) Electric fields monitored at 8 GHz (fundamental frequency) when the input frequency is 8 GHz. (b) Electric fields monitored at 16 GHz (second harmonic) when the input frequency is 8 GHz. (c) Electric fields monitored at 10 GHz (fundamental frequency) when the input frequency is 10 GHz. (d) Electric fields monitored at 20 GHz (second harmonic) when the input frequency is 10 GHz.

which is composed of a planar platform, an Agilent VNA (N5230C), an Agilent signal generator (E8257D), a detector, and a motion controller. The fabricated active sample is put on the planar platform, which can move in the  $x$ - and  $y$ -directions automatically controlled by the motion controller. The input port of the SPP waveguide is connected to the signal generator through SMA to feed the EM energy, an electric-monopole detector is connected to one port of the VNA to probe the vertical components of the electric fields, and two broadband matching loads are connected to the other port of the VNA and the output port of the active SPP waveguide, respectively. Then we obtain the near-electric-field scanning on the measurement plane with a step resolution of 0.5 mm. The measured near-field distributions at different frequencies are illustrated in Figure 6, in which (a) and (b) illustrate the electric fields at the fundamental frequency of 8 GHz and second harmonic of 16 GHz, while (c) and (d) present the electric fields at a fundamental frequency of 10 GHz and a second harmonic of 20 GHz. In both cases, we clearly observe the generations of second-harmonic SPPs through a subwavelength-scale active chip from the measured near fields, which propagate very well to the output port.

In summary, we proposed to generate the second-harmonic spoof SPPs with significant gains using a subwavelength-scale nonlinear chip in broadband microwave frequencies. To incorporate the nonlinear chip efficiently, we adopted two corrugated metallic strips that are printed on the top and bottom surfaces of a dielectric substrate antisymmetrically. Through the nonlinear active chip, we realized second-harmonic generations of SPPs experimentally, in which the measured conversion gains are around 10 from 6 to 10 GHz, having good agreement with the theoretical analysis. We also directly measured the second-harmonic SPPs from the near electric fields.

Considering the high efficiency and excellent performance, the second-harmonic generator can be used as an SPP frequency multiplier in real applications. Especially, the feature of the high gain is beneficial for the SPP circuits and systems because of the ability of solving the loss-associated problem.

Meanwhile, the proposed method can be directly extended to produce higher-order harmonics of SPPs in the microwave frequency, realizing high-performance SPP mixers. We may also use the method to generate SPP multipliers and mixers at millimeter wavelengths and terahertz frequencies.

Compared to devices based on traditional transmission lines (e.g., microstrip),<sup>44</sup> the spoof SPP waveguide has been demonstrated as a potential solution to solve the challenge of signal integrity.<sup>45</sup> So, the proposed spoof SPP multiplier has an advantage in large-scale high-density circuits. Especially, for the terahertz range, by virtue of a Cherenkov radiation source based on SPPs,<sup>46</sup> it is possible to achieve a higher frequency and more powerful source. Although this method cannot be directly applied in optical regimes due to the limit of the speed of electron mobility of a conventional semiconductor, which limits the application of FETs at optical frequencies, according to some brilliant research on new materials, such as black phosphorus,<sup>47</sup> graphite,<sup>48</sup> and silicene,<sup>49</sup> this limit may be broken in the near future. So this method may have an effect on the optical regimes with the aid of new-type FETs made of new materials. Together with other active and passive SPP components,<sup>19,43,50–56</sup> the presented work provides a promising basis to build large-scale SPP integrated circuits and systems in the microwave and terahertz regimes.

## ■ AUTHOR INFORMATION

### Corresponding Author

\*E-mail: [tjcui@seu.edu.cn](mailto:tjcui@seu.edu.cn).

### Notes

The authors declare no competing financial interest.

## ■ ACKNOWLEDGMENTS

H.C.Z. and T.J.C. contributed equally to this work. This work was supported in part from the National Natural Science Foundation of China under Grant Nos. 61138001, 61171024, 61171026, 61302018, 61401089, 61401091, 61571117, 61501112, and 61501117, in part from the National Instrumentation Program under Grant No. 2013YQ200647, and in part from the 111 Project under Grant No. 111-2-05.

## ■ REFERENCES

(1) Barnes, W. L.; Dereux, A.; Ebbesen, T. W. Surface Plasmon Subwavelength Optics. *Nature* **2003**, *424*, 824–830.

(2) Shin, H.; Fan, S. H. All-angle Negative Refraction for Surface Plasmon Waves Using a Metal-Dielectric-Metal Structure. *Phys. Rev. Lett.* **2006**, *96*, 073907.

(3) Hutter, E.; Fendler, J. H. Exploitation of Localized Surface Plasmon Resonance. *Adv. Mater.* **2004**, *16*, 1685–1706.

(4) Yin, L. L.; Vlasko-Vlasov, V. K.; Pearson, J.; Hiller, J. M.; Hua, J.; Welp, U.; Brown, D. E.; Kimball, C. W. Subwavelength Focusing and Guiding of Surface Plasmons. *Nano Lett.* **2005**, *5*, 1399–1402.

(5) Schuller, J. A.; Barnard, E. S.; Cai, W.; Jun, Y. C.; White, J. S.; Brongersma, M. L. Plasmonics for Extreme Light Concentration and Manipulation. *Nat. Mater.* **2010**, *9*, 193–204.

(6) Maier, S. A.; Brongersma, M. L.; Kik, P. G.; Meltzer, S.; Requicha, A. A. G.; Atwater, H. A. Plasmonics-A Route to Nanoscale Optical Devices. *Adv. Mater.* **2001**, *13*, 1501–1505.

(7) Aubry, A.; Lei, D. Y.; Fernandez-Domínguez, A. I.; Sonnemann, Y.; Maier, S. A.; Pendry, J. B. Plasmonic Light-Harvesting Devices Over the Whole Visible Spectrum. *Nano Lett.* **2010**, *10*, 2574–2579.

(8) Jones, A. C.; Olmon, R. L.; Skrabalak, S. E.; Wiley, B. J.; Xia, Y. N.; Raschke, M. B. Mid-IR Plasmonics: Near-Field Imaging of Coherent Plasmon Modes of Silver Nanowires. *Nano Lett.* **2009**, *9*, 2553–2558.

(9) Fang, N.; Lee, H.; Sun, C.; Zhang, X. Sub-Diffraction-Limited Optical Imaging with a Silver Superlens. *Science* **2005**, *308*, 534–537.

(10) Zhang, S.; Xiong, Y.; Bartal, G.; Yin, X.; Zhang, X. Magnetized Plasma for Reconfigurable Sub-Diffraction Imaging. *Phys. Rev. Lett.* **2011**, *106*, 243901.

(11) Schmidt, M. A.; Lei, D. Y.; Wondraczek, L.; Nazabal, V.; Maier, S. A. Hybrid Nanoparticle-Microcavity-Based Plasmonic Nanosensors with Improved Detection Resolution and Extended Remote-Sensing Ability. *Nat. Commun.* **2012**, *3*, 1108.

(12) Luk'yanchuk, B.; Zheludev, N. I.; Maier, S. A.; Halas, N. J.; Nordlander, P.; Giessen, H.; Chong, C. T. The Fano Resonance in Plasmonic Nanostructures and Metamaterials. *Nat. Mater.* **2010**, *9*, 707–715.

(13) Anker, J. N.; Hall, W. P.; Lyandres, O.; Shah, N. C.; Zhao, J.; Van Duyne, R. P. Biosensing with Plasmonic Nanosensors. *Nat. Mater.* **2008**, *7*, 442–453.

(14) Polman, A.; Atwater, H. A. Photonic Design Principles for Ultrahigh-Efficiency Photovoltaics. *Nat. Mater.* **2012**, *11*, 174–177.

(15) Wang, B.; Zhang, X.; Yuan, X.; Teng, J. Optical Coupling of Surface Plasmons Between Graphene Sheets. *Appl. Phys. Lett.* **2012**, *100*, 131111.

(16) Liu, H.; Wang, B.; Ke, L.; Deng, J.; Chum, C. C.; Teo, S. L.; Shen, L.; Maier, S. A.; Teng, J. High Aspect Sub-diffraction-limit Photolithography Via a Silver Superlens. *Nano Lett.* **2012**, *12*, 1549–1554.

(17) Liu, N.; Wen, F.; Zhao, Y.; Wang, Y.; Nordlander, P.; Halas, N. J.; Alù, A. Individual Nano-Antennas Loaded with Three-Dimensional Optical Nano-circuits. *Nano Lett.* **2013**, *13*, 142–147.

(18) Zhang, S.; Genov, D. A.; Wang, Y.; Liu, M.; Zhang, X. Plasmon-Induced Transparency in Metamaterials. *Phys. Rev. Lett.* **2008**, *101*, 047401.

(19) Zhang, J.; Xiao, S.; Wubs, M.; Mortensen, N. A. Surface Plasmon Wave Adapter Designed with Transformation Optics. *ACS Nano* **2011**, *5*, 4359–4364.

(20) Pendry, J.; Martin-Moreno, L.; Garcia-Vidal, F. Mimicking Surface Plasmons with Structured Surfaces. *Science* **2004**, *305*, 847–848.

(21) Hibbins, A. P.; Evans, B. R.; Sambles, J. R. Experimental Verification of Designer Surface Plasmons. *Science* **2005**, *308*, 670–672.

(22) Garcia-Vidal, F. J.; Martin-Moreno, L.; Pendry, J. B. Surfaces with Holes in Them: New Plasmonic Metamaterials. *J. Opt. A: Pure Appl. Opt.* **2005**, *7*, S97.

(23) Williams, C. R.; Andrews, S. R.; Maier, S. A.; Fernandez-Domínguez, A. I.; Martin-Moreno, L.; Garcia-Vidal, F. J. Highly Confined Guiding of Terahertz Surface Plasmon Polaritons on Structured Metal Surfaces. *Nat. Photonics* **2008**, *2*, 175–179.

(24) Maier, S. A.; Andrews, S. R.; Martin-Moreno, L.; Garcia-Vidal, F. J. Terahertz Surface Plasmon-Polariton Propagation and Focusing on Periodically Corrugated Metal Wires. *Phys. Rev. Lett.* **2006**, *97*, 176805.

(25) Atwater, H. A.; Polman, A. Plasmonics for Improved Photovoltaic Devices. *Nat. Mater.* **2010**, *9*, 205–213.

(26) Nagpal, P.; Lindquist, N. C.; Oh, S.-H.; Norris, D. J. Ultrasmooth Patterned Metals for Plasmonics and Metamaterials. *Science* **2009**, *325*, 594–597.

(27) Zhou, Y. J.; Jiang, Q.; Cui, T. J. Bidirectional Bending Splitter of Designer Surface Plasmons. *Appl. Phys. Lett.* **2011**, *99*, 111904.

(28) Rivas, J. G. Terahertz: The Art of Confinement. *Nat. Photonics* **2008**, *2*, 137–138.

(29) Gan, Q.; Fu, Z.; Ding, Y. J.; Bartoli, F. J. Ultrawide-Bandwidth Slow-Light System Based on THz Plasmonic Graded Metallic Grating Structures. *Phys. Rev. Lett.* **2008**, *100*, 256803.

(30) Shen, X.; Cui, T. J.; Martin-Cano, D. F.; Garcia-Vidal, J. Conformal Surface Plasmons Propagating on Ultrathin and Flexible Films. *Proc. Natl. Acad. Sci. U. S. A.* **2013**, *110*, 40–45.

(31) Kauranen, M.; Zayats, A. V. Nonlinear Plasmonics. *Nat. Photonics* **2012**, *6*, 737–748.

(32) Zharov, A. A.; Shadrivov, I. V.; Kivshar, Y. S. Nonlinear Properties of Left-Handed Metamaterials. *Phys. Rev. Lett.* **2003**, *91*, 037401.

(33) Tassin, P.; Van der Sande, G.; Veretenov, N.; Kockaert, P.; Veretennicoff, I.; Tlidi, M. Three-dimensional structures in nonlinear cavities containing left-handed materials. *Opt. Express* **2006**, *14*, 9338.

(34) Shadrivov, I. V.; Kozyrev, A. B.; van der Weide, D. W.; Kivshar, Y. S. Tunable Transmission and Harmonic Generation in Nonlinear Metamaterials. *Appl. Phys. Lett.* **2008**, *93*, 161903.

(35) Kozyrev, A. B.; van der Weide, D. W. Nonlinear Left-Handed Transmission Line Metamaterials. *J. Phys. D: Appl. Phys.* **2008**, *41*, 173001.

(36) Shadrivov, I. V.; Morrison, S. K.; Kivshar, Y. S. Tunable Split-Ring Resonators for Nonlinear Negative-Index Metamaterials. *Opt. Express* **2006**, *14*, 9344.

(37) Wang, B.; Zhou, J.; Koschny, T.; Soukoulis, C. M. Nonlinear Properties of Split-Ring Resonators. *Opt. Express* **2008**, *16*, 16058.

(38) Poutrina, E.; Huang, D.; Smith, D. R. Analysis of Nonlinear Electromagnetic Metamaterials. *New J. Phys.* **2010**, *12*, 093010.

(39) Wurtz, G. A.; Zayats, A. V. Nonlinear Surface Plasmon Polaritonic Crystals. *Laser Photonics Rev.* **2008**, *2*, 125.

(40) Wurtz, G. A.; Pollard, R.; Zayats, A. V. Optical Bistability in Nonlinear Surface-Plasmon Polaritonic Crystal. *Phys. Rev. Lett.* **2006**, *97*, 057402.

(41) Grosse, N. B.; Heckmann, J.; Woggon, U. Nonlinear Plasmon-Photon Interaction Resolved by k-Space Spectroscopy. *Phys. Rev. Lett.* **2012**, *108*, 136802.

(42) Quail, J. C.; Rako, J. G.; Simon, H. J.; Deck, R. T. Optical Second-Harmonic Generation with Long-Range Surface Plasmons. *Phys. Rev. Lett.* **1983**, *50*, 1987.

(43) Zhang, H. C.; Liu, S.; Shen, X.; Chen, L. H.; Li, L.; Cui, T. J. Broadband Amplification of Spoof Surface Plasmon Polaritons at Microwave Frequencies. *Laser&Photon. Rev.* **2015**, *9*, 83–90.

(44) O'Ciardha, E.; Lidholm, S. U.; Lyons, B. Generic-Device Frequency-Multiplier Analysis—a Unified Approach. *IEEE Trans. Microwave Theory Tech.* **2000**, *48*, 1134.

(45) Zhang, H. C.; Cui, T. J.; Zhang, Q.; Fan, Y.; Fu, X. Breaking the Challenge of Signal Integrity Using Time-Domain Spoof Surface Plasmon Polaritons. *ACS Photonics* **2015**, *2*, 1333–1340.

(46) Liu, S.; Zhang, P.; Liu, W.; Gong, S.; Zhong, R.; Zhang, Y.; Hu, M. Surface Polariton Cherenkov Light Radiation Source. *Phys. Rev. Lett.* **2012**, *109*, 153902.

(47) Li, L.; Yu, Y.; Ye, G. J.; Ge, Q.; Ou, X.; Wu, H.; Feng, D.; Chen, X. H.; Zhang, Y. Black Phosphorus Field-Effect Transistors. *Nat. Nanotechnol.* **2014**, *9*, 372–377.

(48) Burghard, M.; Klauk, H.; Kern, K. Carbon-Based Field-Effect Transistors for Nanoelectronics. *Adv. Mater.* **2009**, *21*, 2586.

(49) Jose, D.; Datta, A. Structures and Electronic Properties of Silicene Clusters: A Promising Material for FET and Hydrogen Storage. *Phys. Chem. Chem. Phys.* **2011**, *13*, 7304–7311.

(50) Yang, Y.; Chen, H.; Xiao, S.; Mortensen, N. A.; Zhang, J. Ultrathin 90-Degree Sharp Bends for Spoof Surface Plasmon Polaritons. *Opt. Express* **2015**, *23*, 241242.

(51) Ma, H. F.; Shen, X.; Cheng, Q.; Jiang, W. X.; Cui, T. J. Broadband and High-Efficiency Conversion from Guided Waves to Spoof Surface Plasmon Polaritons. *Laser & Photon. Rev.* **2014**, *8*, 146–151.

(52) Shen, X.; Cui, T. J. Planar Plasmonic Metamaterial on a Thin Film with Nearly Zero Thickness. *Appl. Phys. Lett.* **2013**, *102*, 211909.

(53) Xu, J. J.; Zhang, H. C.; Zhang, Q.; Cui, T. J. Efficient Conversion of Surface-Plasmon-Like Modes to Spatial Radiated Modes. *Appl. Phys. Lett.* **2015**, *106*, 021102.

(54) Shen, X.; Cui, T. J. Ultrathin Plasmonic Metamaterial for Spoof Localized Surface Plasmons. *Laser & Photon. Rev.* **2014**, *8*, 137–145.

(55) Huidobro, P. A.; Shen, X.; Cuerda, J.; Moreno, E.; Martin-Moreno, L.; Garcia-Vidal, F. J.; Cui, T. J.; Pendry, J. B. Magnetic Localized Surface Plasmons. *Phys. Rev. X* **2014**, *4*, 021003.

(56) Pan, B. C.; Liao, Z.; Zhao, J.; Cui, T. J. Controlling Rejections of Spoof Surface Plasmon Polaritons Using Metamaterial Particles. *Opt. Express* **2014**, *22*, 13940.